HHS Public Access

Author manuscript

Biochemistry. Author manuscript; available in PMC 2020 November 12.

Published in final edited form as:

Biochemistry. 2019 November 12; 58(45): 4505–4518. doi:10.1021/acs.biochem.9b00507.

Divalent cations and the divergence of $\beta\gamma$-crystallin function.

Kyle Roskamp[†], **Natalia Kozlyuk**[†], **Suvrajit Sengupta**[†], **Jan C. Bierma**[‡], **Rachel W. Martin**[†,‡]

[†]Department of Chemistry, University of California, Irvine, CA 92697-2025, USA

[‡]Department of Molecular Biology and Biochemistry, University of California, Irvine, CA 92697-3900, USA

Abstract

The $\beta\gamma$-crystallin superfamily contains both the β- and γ-crystallins of the vertebrate eye lens and the microbial calcium-binding proteins, all of which are characterized by a common double-Greek key domain structure. The vertebrate $\beta\gamma$-crystallins are long-lived structural proteins that refract light onto the retina. In contrast, the microbial $\beta\gamma$-crystallins bind calcium ions. The $\beta\gamma$-crystallin from the tunicate *Ciona intestinalis* (*Ci*-$\beta\gamma$) provides a potential link between these two functions: it binds calcium with high affinity and is found in a light-sensitive sensory organ that is highly enriched in metal ions. Thus *Ci*-$\beta\gamma$ is valuable for investigating the evolution of the $\beta\gamma$-crystallin fold away from calcium binding and toward stability in the apo form as part of the vertebrate lens. Here we investigate the effect of Ca^{2+} and other divalent cations on the stability and aggregation propensity of *Ci*-$\beta\gamma$ and human γS-crystallin (H S). Beyond Ca^{2+}, *Ci*-$\beta\gamma$ is capable of coordinating Mg^{2+}, Sr^{2+}, Co^{2+}, Mn^{2+}, Ni^{2+}, and Zn^{2+}, although only Sr^{2+} is bound with comparable affinity to its preferred metalion. The extent to which the tested divalent cations stabilize *Ci*-$\beta\gamma$ structure correlates strongly with ionic radius. In contrast, none of the tested divalent cations improved the stability of HγS, and some of them induced aggregation. Zn^{2+}, Ni^{2+}, and Co^{2+} induce aggregation by interacting with cysteine residues, whereas Cu^{2+}-mediated aggregation proceeds via a different binding site.

Introduction

The vertebrate β- and γ-crystallins are structural proteins that make up the refractive tissue of the eye lens, where they compose up to 50% of the dry weight. Their extraordinary solubility enables them to pack at concentrations of more than 350 mg/mL in the lenses of humans and 750 mg/mL in those of fish. These strongly conserved proteins contain two or more $\beta\gamma$-crystallin domains, a β-sandwich structure comprising two sequential Greek key motifs, and are thought to share a common ancestor with the Ca^{2+}-binding $\beta\gamma$-crystallins found in microbes and invertebrates. Microbial $\beta\gamma$-crystallins contain a characteristic double clamp Ca^{2+}-binding motif in which the loops situated atop the protein contribute binding

rachel.martin@uci.edu.

Supporting Information

The associated Supplementary Information contains additional biophysical characterization and sequence analysis data.

Accession Codes

Uniprot CRYGS_HUMAN, F6Q2R9_CION

residues to both sites. The idea that vertebrate lens crystallins evolved from calcium-binding $\beta\gamma$-crystallins, based on structural homology, is well attested in the literature on lens protein evolution.[1,2] The *Ci-*$\beta\gamma$ crystallin from the tunicate *Ciona intestinalis* appears to bridge both crystallin functions: it is expressed in the papillae as well as the sensory vesicle, a structure found in ascidians that contains the gravity-sensing otolith and the light-sensitive ocellus.[3] A tunicates begins life as a free-swimming larva resembling a tadpole. During this larval stage, the animal navigates its environment using sensory inputs from the otolith and the ocellus.[4] Once it reaches the appropriate developmental stage, the tunicate attaches to a suitable substrate location via an adhesive secreted by the papillae.[5] The expression of *Ci-*$\beta\gamma$ in both of these organs (and nowhere else)[6] underscores the significance of its dual role, representing a transition between the microbial calcium-binding crystallins and the vertebrate lens crystallins. *Ci-*$\beta\gamma$ contains two functional double clamp Ca^{2+}-binding sites and is also more highly refractive than its amino acid composition alone would suggest (although to a lesser extent than vertebrate lens proteins),[7] further suggesting dual functionality.

Despite their similar ancestry,[8,9] many of the vertebrate $\beta\gamma$-crystallins appear to have eschewed calcium binding activity,[10] possibly as a result of their evolution to the more stable two domain structures, or simply through genetic drift.[11] Some reports have suggested that the lens β- and γ-crystallins weakly interact with calcium;[12,13] however, NMR chemical shift perturbation suggests no structural changes upon addition of Ca^{2+} for human γS-crystallin.[14] Moonlighting is seemingly omnipresent for vertebrate taxon-specific crystallins, including δ- (argininosuccinate lyase),[15] ε- (lactate dehydrogenase),[16] ζ- (quinone reductase),[17] λ-(3-hydroxyacyl-CoA dehydrogenase),[18] and τ- (α-enolase),[19] as a variety of small, soluble proteins were recruited to the lens via gene duplication, raising the possibility that the ubiquitous vertebrate $\beta\gamma$-crystallins may have also retained cation-binding functionality.

The interactions of $\beta\gamma$-crystallins with divalent cations have important implications for lens homeostasis and cataractogenesis. For example, copper and zinc ions increase the chaperone activity of the lens α-crystallins, but become displaced upon substrate binding.[20] Incubation of free zinc and copper with γD-crystallin results in the formation of light scattering aggregates,[21,22] thus a positive feedback cycle could exacerbate cataract fromation. Moreover, elemental analysis of cataract and diabetic lenses has shown that elevated levels of copper are present.[23,24] Likewise, elevated levels of cadmium, iron, zinc and other metals have been reported in cataract by several groups.[25–27] Increased metal ion concentration in the lens could promote γ-crystallin aggregation directly[28] or indirectly through the displacement of copper from α-crystallins. In prion and other protein aggregation diseases, the displacement of copper alters protein-protein interactions and inhibits protein function.[29]

In contrast to the vertebrate γ-crystallins, which appear not to have significant cation interactions in the healthy lens, the cation-binding $\beta\gamma$-crystallins such as M-crystallin,[30] clostrillin,[31] rhodollin,[31] spherulin,[32] and protein S[33] exhibit dramatically increased thermal and chemical stability in the presence of calcium ions. These changes are often concomitant with binding-induced structural changes. The $\beta\gamma$-crystallin from *Ciona intestinalis* (*Ci-*$\beta\gamma$), is primarily found in the calcium carbonate-rich matrix of the otolith located above the

photoreceptive ocellus. In addition to its location in a lens-like organ, the *Ci-βγ*-crystallin gene promoter is functional in transgenic vertebrate assays, suggesting that it is a close homolog of the lens *βγ*-crystallins.[34] Unlike many other cation-binding *βγ*-crystallin domains, which are found within a higher molecular weight protein, *Ci-βγ* has only a single domain. For these reasons, *Ci-βγ* is an ideal candidate for investigating stability differences between the lens *γ*-crystallins and cation-binding *βγ*-crystallins.

In the Ca^{2+}-binding EF-hand motif of calmodulin[35] and ion channels,[36,37] other divalent cations may compete with Ca^{2+} at its binding site. In fish otolith and lenses, environmentally common cations such as Sr^{2+} and Fe^{2+} are present in addition to trace metals including Mn^{2+}, Co^{2+}, and Pb^{2+}.[38] The effect of non-calcium cation binding on these proteins' structure and stability, however, remains incompletely characterized. Similarly, limited research has been conducted on the effect of non-oxidizing cations on lens *βγ*-crystallin interactions and stability. Understanding the similarities and differences between these crystallin subgroups beyond their overall structural fold is paramount to understanding the evolutionary development of lens protein stability. Moreover, a comparative analysis is also necessary for elucidating how exogenous factors influence *βγ*-crystallin behavior and to characterize the functional range of the crystallin double-clamp binding motif. In order to address these questions, we have investigated the effect of the divalent cations of magnesium, calcium, strontium, manganese, cobalt, nickel, zinc, and copper on the stability of human *γ*S-crystallin (H*γ*S) and *Ciona intestinalis βγ*-crystallin (*Ci-βγ*). We have also performed structural and sequence analysis of lens and cation-binding *βγ*-crystallins to place these experimental observations in an evolutionary context.

Materials and methods

Amino acid composition analysis

The DNA sequences of lens *γ*-crystallins were collected from NCBI (https://www.ncbi.nlm.nih.gov/protein) searches using the keywords "gamma crystallin", "beta crystallin S", "beta gamma crystallin", "betagamma crystallin" and filtered for 'Animals' and sequences between 170 and 185 residues. Low-quality, crystallin-like, homolog, related, point mutant, partial, and incomplete sequences were removed by manual review of each entry. Leading methionine residues were removed from applicable sequences. To avoid overweighting, only one paralog of polymorphic *γ*-crystallins was used in the final data set. To maintain similarity to the experimentally characterized human *γ*S-crystallin, only *γ*-crystallin sequences from terrestrial vertebrates were analyzed. The final data set was composed of 50 *γ*A-, 78 *γ*B-, 62 *γ*C-, 55 *γ*D- and 62 *γ*S-crystallins. Additionally, the DNA sequences corresponding to the 7 *βγ*-crystallin proteins for which PDB structures confirm cation-binding coordination through the double clamp binding motif (PDBID: 1HDF,[39] PDBID: 1NPS,[33] PDBID: 2BV2,[6] PDBID: 3HZB,[31] PDBID: 3HZ2,[31] PDBID: 3I9H,[31] and PDBID: 4IAU[40]) were collected from the NCBI database. *γ*E-, *γ*F-, and *γ*N-crystallins were excluded from this study because they are either not expressed or are pseudogenes in humans.

Sequence alignments and selection analysis

The alignments for all DNA and protein sequences were generated using MEGA7.[41] Protein sequences were aligned using MUSCLE with default gap penalties and the UPGMB clustering matrix.[42] Trees for each alignment were then constructed from the DNA of the aligned protein sequences using the neighbor-joining method. Preliminary dN/dS calculations for selection at each codon were subsequently calculated using Felsenstein 1981 (F1981), General Time Reversible (GTR), Hasegawa-Kishino-Yano (HKY), and Tamura-Nei (TN) methods from MEGA7. Further codon selection analysis was also calculated using the Single-Likelihood Ancestor Counting (SLAC) and Fixed Effects Likelihood (FEL) methods using the program HyPhy,[43] which produced identical results.

Solvent-exposed surface area

The side chain solvent-accessible surface area (SASA) for cysteine residues was calculated using VADAR (http://vadar.wishartlab.com/).[44] Structures from the Protein Data Bank were used for γB (PDBID: 2JDF[45]), γC (PDBID: 2NBR[46]), γD (PDBID: 1HK0[47]), and γS (PDBID: 2M3T[48]), whereas an ITASSER model[49] was generated for γA, for which no experimental structure was available.

Protein Expression and Purification

Expression and purification of natural abundance and uniformly ^{15}N-labeled tunicate βγ-crystallin and human γS-crystallin were performed as previously described.[14] Briefly, the genes encoding each protein were cloned into a pET28a(+) vector (Novagen, Darmstadt, Germany) and overexpressed in a Rosetta *E. coli* cell line (DE3) using Studier's autoinduction protocol.[50] Tunicate βγ-crystallin lysate was purified via anion exchange and two runs of size-exclusion chromatography. Human γS-crystallin[1] with an N-terminal 6× His tag and a TEV cleavage sequence (ENLFQG) was purified via nickel affinity chromatography, digestion with TEV protease (produced in-house), subsequent nickel affinity chromatography, and finally, two size exclusion chromatography (SEC) runs. The monomeric and dimeric species were collected separately from the first SEC purification and then subjected to SEC a second time. All samples were dialyzed into metal-free 10 mM HEPES, 0.05 % NaN_3, pH 7.1 unless otherwise stated. Similarly, all samples were reduced via incubation with 5 mM dithiothreitol (DTT) (made fresh) for 30 minutes at RT, dialyzed overnight to remove DTT, and used for measurements immediately thereafter. This procedure was used to prevent the spontaneous dimer formation that can occur at higher concentration in the absence of reducing agent.[51]

Turbidity (Light Scattering)

A Spark TECAN plate reader (Tecan Trading AG, Switzerland) was used to measure light scattering (405 nm) of *Ci*-βγ, HγS-WT and HγS variants in the presence of Cu^{2+} and Zn^{2+} at 30 °C, and Co^{2+} and Ni^{2+} at 42 °C. 200 μL of protein at 50 μM (10 mM HEPES, 50 mM NaCl, pH 7.1) was placed in a 96-well plate and treated with variable equivalents of divalent

[1]Amino acid indices referenced in this paper include the glycine at the first position which is left after TEV cleavage. This glycine is in the position where a start methionine would be, and is often not included in the sequence numbering. The numbering used here therefore differ from some other S-crystallins references by 1.

cation after a 5 minute baseline period. In Zn^{2+} measurements, after two hours, 2, 10, or 20 equivalents (10 μL) of ethylenediaminetetraacetic acid (EDTA) were added to the solution to chelate available cations. Measurements were recorded every 60 seconds with 5 seconds of shaking before readings. The reported measurements were determined by subtracting the absorbance of the buffer measured in parallel. The light scattering observed for the protein-only solution was identical to the buffer-only samples and is omitted for clarity. To minimize potential instrumental bias, the locations of all samples on a plate were assigned at random.

Tryptophan fluorescence

Thermal denaturation was detected via intrinsic tryptophan fluorescence for *Ci-βγ* and HγSWT. 5 μM protein solutions with 50 μM divalent cation ($CaCl_2$, $CoCl_2$, $MgCl_2$, $MnCl_2$, $NiCl_2$, $SrCl_2$, or $ZnCl_2$) or EDTA added were assayed incrementally over a 17–99 °C temperature range. Measurements were acquired using a Varian Cary Eclipse fluorescence spectrophotometer with an excitation wavelength of 280 nm and a 5 nm excitation slit. The sample temperatures were controlled using a Quantum Northwest TC 1 temperature controller (Quantum Northwest, Inc.) with a two minute equilibration at each 1 °C temperature increment. The fraction unfolded was calculated from the 360/320 fluorescence ratio and fit to a two-state equilibrium unfolding model to determine the denaturation midpoint temperature (T_m) of each sample. Fluorescence changes at 330 nm were calculated by subtracting the native protein fluorescence of each sample from the fluorescence following divalent cation addition. Samples were allowed to thermally equilibrate to within instrument sensitivity at 20 °C for two minutes before measurements were made.

The change in intrinsic tryptophan fluorescence was measured for each aforementioned divalent cation. A 1000 μL sample containing 5 μM protein was measured prior to and following the addition of 10 μL of 5 mM divalent cation. Measurements were repeated six times for each divalent cation.

Dynamic light scattering

Thermal gradient dynamic light scattering (DLS) measurements were performed using a Malvern Zetasizer NS for *Ci-βγ* measurements and a Malvern Zetasizer μV for HγS measurements. Each sample was composed of 150 μM protein with 975 μM divalent cation. Experiments were performed at 1 °C increments from 20 to 92 °C with two minute equilibrations before measurements and 1 °C/min temperature ramping between measurements. 10 second correlations were measured six times and repeated three times for each temperature step.

Mass Spectrometry

The insoluble aggregates of HγS-WT and HγS-C_0 with 10 equivalent of $CuCl_2$ were prepared via incubation at 30 °C for 12 hours and collected via centrifugation. Pellets were washed four times with double deionized water, once with 20 equivalents of EDTA, once with 10 mM DTT, and twice more with double deionized water. The samples were then dialyzed into double deionized water to remove urea. 0.5 mg/mL samples of both proteins were digested using MS Grade Pierce Trypsin Protease (ThermoFischer Scientific, Rockford, IL, USA) with or without DTT at 37 °C overnight. A Waters Synapt G2 mass

spectrometer was used to detect the resulting peptide fragments with a 30 minute separation on a Waters I-Class UPLC column. The resulting MS and MSMS data was analyzed using BioPharmaLynx for peptide and post-translational modification identification. HγS-WT and HγS-C_1 digests were only analyzed for cysteine oxidation products. HγS-C_0 and *Ci-*$\beta\gamma$ were probed for PTMs. The following PTMs were searched for based on previously observed modifications in aged and cataractous lenses[52,53] and known radical oxidative products[54,55] : −18 Da (dehydration/succinimide - S,T/N,D), +1 Da (deamidation - N,D or 2-amino-3-oxo-butanoic acid - T), +4 Da (kynurenine - W), +16 Da (oxidation/ hydroxylation - M,C,H,W,F,Y,N,D), +28 Da (carbonylation - S,H,K), +32 Da (dioxidation - C, M), +55 Da (R). Missed trypsin cleavages were required for modified arginine or lysine residues. Only peptides in which at least 35% of b and y ions were observed and for the parent and modified fragments were considered.

Isothermal titration calorimetry

ITC measurements were performed using a MicroCal PEAQ-ITC (Malvern Instruments, Northampton, MA, USA). Each titration consisted of 1.5 μL injections of 2 mM (Ca_2, $SrCl_2$) or 5 mM (Mg_2, Mn_2, Co_2, Ni_2, Zn_2) cation solution to a 200 μM protein sample in 10 mM HEPES (pH 7). Injections were made every 180 seconds for $CaCl_2$ and $SrCl_2$. The remaining samples had the initial 10 injections made every 300 seconds and every 200 seconds for the remaining injection In total, 25 titrations were performed. To control for the heat of dilution, 10 mM divalent cation was titrated into 10 mM HEPES and the resulting data were subtracted from the raw protein data. The ITC data were initially analyzed using Mathematica as previously described[14] to obtain reasonable initial values and then fit to a two-state binding model using MicroCal PEAQ-ITC Analysis Software. The reported fit parameters are the mean of two trials, while the error bars represent one standard deviation.

Solution-state NMR spectroscopy

Experiments were performed at 25 °C on a Varian *Unity*INOVA system operating at 800 MHz proton Larmor frequency and equipped with a $^1H/^{13}C/^{15}N$ 5 mm tri-axis PFG triple-resonance probe. 15N-^{1}H HSQC experiments were acquired with 4 scans in the direct dimension and 64 scans in the indirect dimension at protein concentrations of 1.7 mM in the presence of 1, 2, and 6.5 equivalents of $MgCl_2$, $NiCl_2$, $ZnCl_2$, or $SrCl_2$. Chemical shift perturbations (CSP) were calculated using the following equation:

$\Delta\delta_{avg} = \sqrt{\frac{\left(\Delta\delta_N/5\right)^2 + \left(\Delta\delta_H\right)^2}{2}}$. Chemical shift perturbation thresholds for strong (CSP ≥ 0.2 ppm) and moderate (0.2 < CSP ≥ 0.06 ppm) were based on the chemical shift perturbation reported previously for *Ci-*$\beta\gamma$ interactions with Ca^{2+}.[14] CSP less than 0.06 ppm was classified as unperturbed.

Far-UV circular dichroism

The far-UV circular dichroism (CD) spectra of 5 μM HγS were measured on a J-810 spectropolarimeter (JASCO, Easton, MD). Spectra were recorded from 250 nm to 195 nm using a 1 nm bandwidth and 4 s response.

Results and Discussion

Vertebrate lens and cation-binding βγ-crystallins differ in amino acid composition

Irrespective of function, all βγ-crystallins are topologically similar. One important conserved feature is an (F/Y/W)xxxx(F/Y)xG motif in the first two β-strands of each Greek key (Figure 1). Additionally, disabled versions of the (N/D)(N/D)xx(T/S)S Ca^{2+}-sequence characteristic of cation-binding βγ-crystallins are readily evident in vertebrate lens γ-crystallins. Point mutations in either motif can compromise protein solubility and result in cataract.[56–60] In particular, reintroduction of Ca^{2+} binding ability in lens γ-crystallins reduces protein stability,[2,61,62] raising questions about how vertebrate lens proteins evolved from their metal-binding ancestors. In order to assess the conservation of residues associated with divalent cation binding during crystallin evolution, the amino acid sequences of cation-binding βγ-crystallins were compared to those of terrestrial vertebrate lens γA-, B-, C-, D-, and S-crystallins. For this analysis, γA-D crystallins were clustered together based on known similarities in gene structure, conservation, and sequence,[63,64] while γS-crystallins were analyzed separately.

One notable difference between the lens and cation-binding βγ-crystallins is in the numbers of positively and negatively charged residues. Cation-binding βγ-crystallins have a net negative charge to aid in the sequestration of cations. In particular, *Ci*-βγ lacks positively charged residues in the vicinity of the Ca^{2+} binding sites; however, this feature is not strongly conserved among other cation-binding βγ-crystallins. The lens γ-crystallins contain similar levels of positively and negatively charged residues, with charged residues evenly dispersed across the protein's surface. On average, lens γ-crystallins contain similar total levels of arginine and lysine (γA-D: 12.9 ± 0.8%, γS: 12.4 ± 0.8%), histidine (γA-D: 3.2 ± 1.0%, γS:3.2 ± 0.8%), and acidic residues (γA-D: 12.8 ± 0.6%, γS: 13.5 ± 0.4%) (Figure 2, Supplementary Table S1). Cation-binding βγ-crystallins contain comparable levels of negatively charged residues (βγ: 11.5 ± 2.6%) but lower levels of arginine and lysine residues (βγ: 8.2 ± 2.5%). Similarly, low levels of histidine (0.7 ± 0.6%), cysteine (0.5 ± 0.9%), and methionine (0.6 ± 0.9%) are found in the cation-binding crystallins. This observation is unsurprising, as cysteine and histidine are the most commonly observed residues in protein metal binding sites and are therefore expected to be localized to the binding sites and hence rare overall.[65] Furthermore, cysteine and methionine are readily oxidizable: post-translational modifications at these sites could result in structural changes, either reducing the stability of the *apo*- form or the binding affinity in the *holo*- form. Despite their similar net charges, the γA-D and γS-crystallins differ substantially in the distribution of positively-charged residues between lysine and arginine. On average, γA-D-crystallins have a 17:2 arginine to lysine ratio compared to the 3:2 ratio observed in the γS-crystallins. This difference may be driven in part by the higher refractivity of arginine, as γA-D-crystallins are located in the more highly refractive lens nucleus, while γS-crystallins are more abundant in the cortex.[66]

Solvent-exposed cysteines are strongly conserved in lens crystallins but not calcium-binding crystallins

Methionine, cysteine, and histidine are more common in lens γ-crystallins than calcium-binding crystallins, consistent with their high refractivity. Methionine is particularly abundant in fish γM-crystallins, many of which contain up to 15% methionine.[67] Overall, the refractive function of lens proteins leads to their being enriched in polarizable amino acids.[68] Here, both groups of lens γ-crystallins are enriched in highly refractive amino acids relative to their metal-binding counterparts (Supplementary Figure S1), consistent with the measured difference in *dn/dc* values for human γS (0.2073) and *Ci-βγ* (0.1985).[7] Relative to side-chain size, cysteine is the most refractive whereas alanine is the least of any amino acid (Supplementary Figure S2), leading to the hypothesis that cysteine plays a critical functional role in the highly refractive lens crystallins. This idea is supported by the sequence data, which indicate that many cysteine residues found in lens γ-crystallins are replaced by other residues in cation-binding crystallins (Supplementary Table S2.) In contrast to cation-binding βγ-crystallins, where the few cysteines present are usually found in disulfide bonds, lens proteins have free, solvent-exposed cysteines (Supplementary Table S3–S4) whose function is not fully understood. Although serine is the most common alternate residue at consensus cysteine positions, a variety of amino acids are observed at the homologous positions in other γ-crystallins (Supplementary Table S2).

In lens γ-crystallins, several conserved cysteine positions are found, predominately in the N-terminal domain (Supplementary Table S5). For both domains, the cysteines closest to one another in space are located in and around the third β-strand. The most concentrated locus of conserved cysteines is found in the N-terminal domain of HγS. C23 and C27 are the closest cysteine pair in this region, and are both spatially adjacent to C25 and C83 (Figure 3). The location of C23, C25, C27 across the second and third β-strands of the first Greek key results in high solvent accessibility—21%, 77%, and 40% respectively—for each side chain. Both of these features, close proximity and high solvent accessibility, were noted by Thorn et al. as factors enabling this triad to drive the formation of domain-swapped dimers.[51] Across the lens γA-D crystallins, the homologous positions to C23 and C83 are similarly occupied by cysteines. The position homologous to C27 is the most conserved position across both domains of the lens γ-crystallins, and is replaced by a histidine only in the N-terminal domain of γD, while the C25 position is unique to the γS-crystallins.

The apparent functional significance of these conserved cysteine residues raises questions about the underlying selection process. Although these residues are highly refractive, they are also capable of non-native intermolecular disulfide bond formation that can lead to aggregation, complicating their utility in an environment where solubility is just as critical as refractivity. Disulfide exchange in human lens γ-crystallins has recently been proposed to help regulate the local redox potential of the lens,[69] however, inter- and intramolecular disulfide bonding has also been shown to facilitate domain swapping in γS-crystallin, providing a possible nucleation site for the formation of deleterious aggregates.[51] Cysteines from each γ-crystallin have also been identified as sites for post-translational modifications in aged lenses,[52,70] while the more solvent-exposed cysteines of γD-crystallin have been shown to be the primary contributors to copper-mediated aggregation.[22]

For all conserved cysteine positions we calculated the non-synonymous and synonymous codon substitutions to investigate potential selective pressure. For each γ sequence alignment, a maximum-likelihood phylogenetic reconstruction was performed to enable calculation of the nonsynonymous and synonymous substitution rates via SLAC (Single-Likelihood Ancestor Counting) and FEL (Fixed Effects Likelihood).[71] No positions exhibit evidence of positive (diversifying) selection, while numerous cysteines, particularly in γS-crystallin, exhibit evidence of strong negative (purifying) selection. Compared to the α- and β-crystallins, the γ-crystallins are the most enriched in cysteine. Moreover, in the six human β-crystallins a cysteine is observed at the position homologous to C27 in HγS, with only 15 total cysteines elsewhere. Notably, no substitutions were observed for the codons of γA-C78, C-C108 (human γD numbering convention), and γS-C83 (human γS numbering convention). No evidence of positive selection was observed for any of the sites examined across all lens γ-crystallins. Each of the seven conserved cysteines of the γS-crystallins appear to experience strong negative selection ($p \leq 0.05$), while ~20% of γA-D crystallins experience similar selection (Supplementary Table S6).

The strong conservation of cysteines in all γ-crystallin sequences and the mutual proximity of the cysteines in the N-terminal domain of γS-crystallin led us to design variants that remove one or more prominently exposed Cys residues in HγS. We hypothesize that if divalent cation interactions are relevant to protein stability or lens homeostasis, mutating C23, C25, and/or C27 would alter cation-binding activity. Therefore, variants with two (HγS-C_2 = γS-C23S/C27S), one, (HγS-C_1 = γS-C23S/C25S/C27S) or zero (HγS-C_0 = γSC23S/C25S/C27S/C115S) solvent-accessible cysteines were produced. For each mutation we chose serine, as oppose to alanine, as a replacement due to its similar size and the observation that it is the most common alternative residue at these sites. The resulting variants also enabled us to more directly compare the behavior of human γS-crystallin and *Ci*-$\beta\gamma$ crystallin, which does not contain cysteine, in the presence of various divalent cations. The results of these experiments are described in subsequent sections.

Ci-$\beta\gamma$ can accommodate a wide range of divalent cations

Unlike better-characterized Ca^{2+} motifs, such as the EF-hand[72,73] or C2-domain,[74] the double clamp motif of $\beta\gamma$-crystallins has not yet been throughly tested for non-Ca^{2+} divalent cation interactions. Previous research has shown Protein S binds Mg^{2+} with one order of magnitude lower affinity,[75] and M-crystallin has been crystallized in the presence of Mg^{2+} (PDBID: 5HT9), however, neither domain of *Yersinia* crystallin interacts with Mg^{2+}.[76] *Ci*-$\beta\gamma$ is a useful $\beta\gamma$-crystallin to investigate non-Ca^{2+} divalent cation binding, due to its high Ca^{2+} affinity, native monomeric form, and the minor asymmetry between its binding sites. Moreover, its native location in a light-sensing organ makes it the best cation-binding $\beta\gamma$-crystallin for comparative analysis with lens γ-crystallins. *Ci*-$\beta\gamma$ binds Ca^{2+} via two-site sequential binding, with high ånity at both sites relative to other $\beta\gamma$-crystallins.[14,62]

Here we used isothermal titration calorimetry (ITC) to investigate the thermodynamics of interactions between *Ci*-$\beta\gamma$ and a variety of divalent cations. The binding isotherms of *Ci*-$\beta\gamma$ to Ca^{2+} and Sr^{2+} were exothermic, while the rest exhibited biphasic behavior. Similar results have been previously reproted for other systems, e.g.[77–79] The extent of exothermic

character of the biphasic isotherms was $Mg^{2+} > Mn^{2+} > Co^{2+} > Ni^{2+} > Zn^{2+}$ (Supplementary Figure S3). The isotherm produced by Sr^{2+} was highly similar to that of Ca^{2+}; the observed data for both cases could be fit to same exothermic two-state model previously reported[14] (Supplementary Figure S4). The binding constants and parameters calculated show slightly stronger binding than we previously reported for *Ci-βγ* to Ca^{2+} in Tris buffer. The overall dissociation constant $\left[K_d = 1/\sqrt{(K_1 K_2)}\right]$ for Ca^{2+} was found to be 0.004 μM and 0.039 μM for Sr^{2+} (Table 1).[14] The identities of the binding sites corresponding to the high and lower affinity binding of Ca^{2+} and Sr^{2+} are not yet known, however we suspect the higher-affinity binding of both cations occurs at the 5-coordinate site and the lower affinity binding occurs at the 4-coordinate site. The two sites are nearly identical, differing only in their third residues. In the first binding site, I33 coordinates cations via its backbone carbonyl whereas the homologous E76 at the second site also coordinates through its sidechain (Figure 1). The sidechain coordination from the third residue of the second binding site in *Ci-βγ* is not observed in any other cation-binding *βγ*-crystallin, which may explain the remarkably high Ca^{2+} affinity of this protein.

Ci-βγ and M-crystallin (36.6%, identity 67.1% similarity via LALIGN[80]) both exhibit similar structural changes upon Ca^{2+} binding, contain two octahedral binding sites, and bind via two-site sequential binding with one order of magnitude difference between sites.[30] A comparison of M-crystallin crystal structures bound to Ca^{2+} (PDBID: 3HZ2[31]) and Mg^{2+} (PDBID: 5HT9) shows that the ligand-cation distances are shorter for Mg^{2+} binding (Supplementary Table S7). The tetrahedral volume between binding site ligands decreases more at the second site from Ca^{2+} and Mg^{2+} binding. The greater reduction in ligand space suggests a greater flexibility at the second binding site. We hypothesize that the second site of *Ci-βγ* is similarly flexible, and would therefore bind with a higher affinity.

Residue-specific interactions of Sr^{2+}, Mg^{2+}, Ni^{2+}, and Zn^{2+} with *Ci-βγ* were investigated using solution-state NMR. ^{1}H-^{15}N HSQC[81] chemical shift perturbations (CSPs) were measured to identify the residues involved in divalent cation interactions (Supplementary Figures S5–S6). Classification of CSP strength was done according to standard threshold levels: (strong ≥ 0.2, moderate ≥ 0.06). Strong and moderate CSPs from the addition of 6.5 equivalents of divalent cation are shown mapped onto the X-ray crystal structures of the Ca^{2+}-bound protein (PDBID: 2BV2)[6] in Figure 4. The regions corresponding to strong CSPs and absent peaks resulting from Sr^{2+}, Mg^{2+}, Ni^{2+}, and Zn^{2+} interactions exhibited distributions that strongly resemble the CSP profile of Ca^{2+}-bound *Ci-βγ*.

For all the divalent cation interactions, strong CSPs were concentrated in the loop regions (31–36 and 72–79) containing three of the four binding moieties for each site (Site 1: I33-O, S35-OG, D75-OD1; Site 2: D32-OD1, E76-O/OE1, S78-OG). The residues completing the binding site motifs (Site 1: E7-O/OE1; Site2: D42-O), located before the *β*-hairpins, also displayed moderate to strong CSPs. Minor CSPs were also observed along the *β*-strands of the Greek keys and in other solvent-exposed surfaces away from the two binding sites for all divalent cations. Notably, above 3 equivalents of metal cation, Ni^{2+} binding resulted in the disappearance of chemical shifts from residues at and adjacent to the calcuim binding site, presumably due to paramagnetic relaxation enhancement, whereas Zn^{2+}, and to a lesser

extent Mg^{2+}, yielded fewer assignable chemical shifts, possibly due to a transition into the intermediate exchange dynamic regime. In general, each tested metal cation interacts strongly with residues composing and adjacent to the Ca^{2+} binding site. Although the ability of Mg^{2+}, Sr^{2+} and various transition metals to coordinate to Ca^{2+} binding sites has been reported for other Ca^{2+}-binding proteins such as calmodulin,[82–84] calcium- and integrin-binding protein,[85,86] and parvalbumin,[87] this represents the first demonstration of a $\beta\gamma$-crystallin coordinating a wide range of non-Ca^{2+} cations.

Divalent cations increase the thermal stability of *Ci-βγ*, but not HγS

Biophysical characterization was performed for *Ci-βγ* and HγS in the presence of a variety of divalent cations to further investigate how the observed composition differences impact protein stability. Thermal unfolding curves were measured for both proteins via the 360/320 nm ratio of tryptophan fluorescence intensities. Tryptophan side-chains in non-polar environments have a peak fluorescence near 320 nm, while those in highly polar environments, e.g. aqueous solution, fluoresce at 360 nm. All tryptophans in the folded structures of *Ci-βγ* and HγS are buried in the hydrophobic core of the protein, therefore, the ratio of fluorescence intensity at 360/320 as a function of temperature is a sensitive marker of protein unfolding, as previously demonstrated for βγ-crystallins.[88,89]

As previously reported, the Ca^{2+}-bound form of *Ci-βγ* has a greatly increased thermal unfolding midpoint (T_m) over the *apo*-form, with a dramatic increase from 46 C to 94 C[14] (Figure 5A). A similar stabilization was observed in the presence of Sr^{2+}, yielding a T_m of 91 °C. Of the tested divalent metal cations, the next greatest T_m was observed for Mn^{2+} (84 °C) followed by Mg^{2+} (71 °C), Co^{2+} (70 °C), Ni^{2+} (61 °C), and Zn^{2+} (53 °C) ((Figure 5B). For the tested cations, a higher T_m was observed to correlate with sharper unfolding transition. The exception to this trend was Zn^{2+}, where the *Ci-βγ* unfolding temperature range is similar to that of the Sr^{2+} and Ca^{2+}-bound forms. The presence of Ca^{2+} did not alter the T_m of HγS ((Figures 5C, 1D), consistent with its previously observed weak binding and lack of changes to NMR chemical shifts upon cation addition.[14] None of the tested divalent cations alter the thermal unfolding behavior of HγS: the T_m was ~72 °C for all samples, consistent with previous literature reports.[90–92]

The wide range of effects on thermal stability of the divalent cations on *Ci-βγ* warrants some discussion of metal ion properties, given that all of these ions have a charge of +2 and are similar in size. Notably, the thermal stabilization from Mn^{2+} is 12–13 °C greater than that due to Mg^{2+}. Examination of different metal ion properties indicates that stabilization *Ci-βγ* correlates most strongly with coordination number, followed by ionic radius (Table 2). In other proteins, the native binding sites of Mn^{2+} and Mg^{2+} are most often BCH and BCB motifs, where binding is predominately coordinated via acid residues.[93] The reduced affinity binding of Mn^{2+} and Mg^{2+} to Ca^{2+} coordination sites has been suggested to stem primarily from differences in ionic radius.[72] A small radius may alter the cation's interaction with some bidentate ligands. A similar argument can be made for Sr^{2+} over Mn^{2+}, despite limited experimental data on Sr^{2+} binding in proteins. Although its ionic radius is slightly larger than that of Ca^{2+}, Sr^{2+} binding results in the same structural changes, with small reductions in ligand-cation coordination. Any minor changes in backbone coordination may

then be accommodated by the flexibility of the aspartate and glutamate residues in the binding site.

Divalent cations alter thermal aggregation in both *Ci-βγ* and HγS

Thermal gradient DLS was used to probe divalent cation-mediated changes in protein-protein interactions leading to the formation of soluble oligomers and insoluble aggregates. In DLS, a translational diffusion coefficient is measured via scattering correlation times, providing a sensitive tool for the detection of oligomer formation. γ-crystallin aggregation under thermal stress often proceeds via a step function in which a sudden onset of oligomerization occurs directly from the monomeric population. We use the notation T_i to refer to the initial temperature at which oligomers or aggregates form from the starting solution of monomers. These early-stage soluble oligomers formed are one to two orders of magnitude larger in size than the monomers or dimers they were derived from. These particles grow in size until they precipitate from solution, resulting in a decrease in scattering intensity, at which point the measurement was terminated.

Thermal unfolding data for *Ci-βγ*, in the apo form and bound to a variety of divalent cations, are shown in Figure 6 A–C. The T_i of *apo-Ci-βγ* occurs near 60 °C, resulting in 20 nm-diameter oligomers. The oligomers remain soluble and increase in diameter to 50 nm at 92 C. Ca^{2+}- and Sr^{2+}-bound *Ci-βγ* exhibit T_i values of 82 °C and 79 °C, respectively, above which the oligomer diameter immediately exceeds 100 nm. The addition of Mg^{2+} to *Ci-βγ* does not alter the T_i (58 °C) relative to the *apo*-form, but yields 35 nm diameter oligomers. The soluble oligomers increase in size with increasing temperature, with 50 nm oligomers forming at 70 °C. Of the tested transition metal cations, only Mn^{2+} significantly increased the T_i of *Ci-βγ*. As observed for Ca^{2+} and Sr^{2+}, oligomers formed at the T_i (70 °C) rapidly exceed the observable size. The addition of Co^{2+}, Ni^{2+}, or Zn^{2+} reduces the T_i of *Ci-βγ*. Co^{2+} reduces the T_i from 60 °C to 55 °C. The oligomers initially formed in the presence of Co^{2+} are 30 nm in diameter and grow to 70 nm by 65 °C, above which the scattering signal is saturated. The T_i values for Ni^{2+} and Zn^{2+} are 50 °C and 40 °C, respectively, where both form relatively small oligomers between 10 nm and 20 nm, with slow growth producing 50 nm oligomers at 70 °C. More rapid increases are observed at higher temperatures.

The analogous data for HγS are presented in Figure 6 D–F. In the absence of divalent cations, HγS rapidly forms insoluble aggregates around 53 °C, consistent with prior studies of HγS alone.[91] The T_i of HγS does not change in the presence of Ca^{2+}, Sr^{2+}, or Mg^{2+}; immediate formation of aggregates is observed in the presence of each of these cations. The transition metal divalent cations Co^{2+} and Ni^{2+} reduced the T_i of HγS, to 50 °C and 46 °C, respectively, whereas Mn^{2+} did not alter the T_i. For all HγS measurements, the aggregate size rapidly exceeded 100 nm. The addition of Zn^{2+} immediately produced large aggregates that precipitated out of solution, therefore, no DLS data are reported for treatment of HγS with this cation. Although *Ci-βγ*-crystallin resists Cu^{2+}-induced aggregation more effectively than γS-WT, upward of six equivalents results in light scattering (Supplementary Figure S7). In comparison, Zn^{2+} similarly aggregates γS-WT, whereas the presence of up to 10-fold Zn^{2+} does not reduce the solubility of *Ci-βγ*. For the variant HγS-C_0, which does

not contain solvent-accessible cysteines, the T_i in the presence of Co^{2+} and Ni^{2+} are both around 49 °C.

Zn^{2+}-driven aggregation of HγS proceeds through cysteine coordination, whereas Cu^{2+}-driven aggregation results from methionine oxidation

In the healthy eye lens, γ-crystallins undergo only weak and transient interactions. Previous studies measuring γ-crystallin interaction with exogenous peptides,[99] small molecules,[100] and cations[21] have highlighted the ability of the lens γ-crystallins to tolerate potentially destabilizing interactions to a certain extent; however this capacity is limited and aggregation results from excessive intermolecular contacts. We therefore focused on changes to protein solubility as a practical approach to determine the potential eėcts of divalent cations on γ-crystallin behavior. The addition of excess Ca^{2+}, Sr^{2+}, Mg^{2+}, and Mn^{2+} did not alter the fluorescence or thermal unfolding of HγS, consistent with previous research demonstrating that HγD-crystallin does not aggregate upon addition of Mn^{2+}, Fe^{2+}, or Ca^{2+},[21,101] and that γB and γS-crystallins do not interact with Ca^{2+}.[14,60] Co^{2+} and Ni^{2+} did not alter the thermal unfolding of HγS, but when present in excess (6.5 fold), produced soluble aggregates under thermal stress, and detectable light scattering after 2 hours at 42 °C (Supplementary Figure S8). The addition of Zn^{2+} results in appreciable aggregation without thermal stress in low excess; therefore, further light scattering measurements were performed on the Cys to Ser variants HγS-C_2, HγS-C_1, and HγS-C_0, which were designed to test the hypothesis that solvent-exposed cysteines are responsible for aggregation-promoting interactions with metal cations in HγS.

At room temperature, aggregates of HγS readily form following the addition of 5 equivalents of Zn^{2+} or 1 equivalent of Cu^{2+}. Characterization of metal-induced aggregation was therefore measured via light scattering at 405 nm. Zinc-induced aggregation of HγS was measured for both the monomeric and dimeric forms (Figure 7). 1 equivalent of Zn^{2+} produced limited aggregation of monomeric HγS, while 5 and 10 equivalents induced elevated levels of light scattering. Upon addition of 10, but not 5, equivalents of Zn^{2+}, a small increase in light scattering of HγS dimers was observed. Similar measurements were performed using monomeric HγS-C_2, HγS-C_1, and HγS-C_0. Similar to HγS-WT, each of the Cys-to-Ser variants produced negligible aggregation in the presence of 1 equivalent of Zn^{2+}. Appreciable γS-C_2 aggregation was observed for the addition of 10 equivalents of Zn^{2+}, while 5 equivalents produced slightly less aggregation. 10 and 5 equivalents of Zn^{2+} yielded similarly low levels of aggregation for γS-C_1, while detectable aggregation of γS-C_0 was only observable at two hours with 10 equivalents. For all proteins and zinc ion equivalents, the addition of EDTA reduced the light scattering intensity to background levels (Figure 7).

The removal of surface-exposed cysteines in HγS-C abrogated Zn^{2+}-mediated aggregation (Figure 7A) as well as Ni^{2+} and Co^{2+}-induced aggregation under mild thermal stress. For all proteins tested, Zn^{2+} aggregation was reversible upon addition of EDTA (Figure 7B), supporting our hypothesis that zinc ions coordinate to HγS via solvent-accessible cysteines and cause intermolecular bridging. Dimerization of HγS, presumably via C25 disulfide bond formation, limits cysteine solvent accessibility. The dramatically reduced aggregation in

HγS dimer-only solutions further supports the idea that cysteine solvent accessibility regulates Zn^{2+}-mediated intermolecular bridging aggregation. Dominguez et al. previously reported that Zn^{2+} induces trace aggregation of HγS, but did not specify the extent of dimerization.[101] Therefore, we suspect that dimerization is responsible for the discrepancy between our results and those reported in this prior study.

Although Hγ-WT aggregates to a greater total extent than HγS-C_2 and HγS-C_1, it does so more slowly. We hypothesize that Zn^{2+} may interact with the more buried C23 (21% SASA) or C27 (40% SASA), resulting in a lesser solvent-accessible surface area for the zinc ion. In this case, the clustered cysteines may serve as a weak buffer against intermolecular bridging. In HγS-C_2 and HγS-C_1, where the remaining solvent-exposed cysteines are not spatially proximal to each other, most of the increase in light scattering occurs immediately. For these two variants, the extent of aggregation is considerably reduced despite a higher ratio of Zn^{2+} to solvent-accessible cysteines.

In addition to Zn^{2+}, we also observed Cu^{2+}-induced aggregation of HγS. The addition of 1 equivalent of Cu^{2+} produced considerable levels of aggregation for HγS-WT and each Cys-to-Ser variant (Supplementary Figure S9), to the extent that precipitation occurred. The dimer of HγS-WT exhibited similar total aggregation under the same conditions. Prior investigations of γD-crystallin have shown that the solvent-accessible residues C109 and C111 are primarily responsible for Cu^{2+}-induced aggregation, which can be blocked using GSSG.[22] ^{1}H-^{15}N HSQC peak intensity disappearances in HγD prepared with Cu2+ provide further evidence that the strongest interactions occur at the solvent accessible-cysteines.[21] We felt confident that the removal of the solvent-accessible cysteines in γS-crystallin, which we observed led to decreased Zn^{2+}-induced aggregation, would have a similar effect for Cu^{2+}. However, this hypothesis proved to be incorrect. In contrast to Zn^{2+}, the removal or reduction of solvent-accessible cysteine side chains does not strongly impact Cu^{2+}-induced aggregation, although the scattering intensity of all samples is decreased upon EDTA addition, suggesting that superficial cross-linking is partially responsible. No changes in protein structure are evident upon the addition of either Cu^{2+} or Zn^{2+} for HγS-WT based on far-UV circular dichroism (Supplementary Figure S10).

To further investigate the mechanism of Cu^{2+}-induced aggregation, we digested the insoluble aggregates of HγS-WT and HγS-C_0 with trypsin to search for oxidative PTMs or modifications observed in aged lenses via mass spectrometry (Supplementary Table S8, Supplementary Figure 11).The light-scattering samples of HγS and HγS-C_0 incubated with 10 equivalents of Cu^{2+} were analyzed via mass spectrometry to determine if post-translational modifications (PTMs) were present. Trypsin digests were performed using the HγS-WT and HγS-C_0 pellets collected via centrifugation with MSMS mapping to confirm PTMs. Mass shifts of +16 Da and +32 Da (corresponding to cysteine oxidation) for peptides containing C23, C25, C27, and C115 were the only modifications investigated from the HγS-WT digest. Across several measurements, MSMS mapping of modification showed C25 was the most consistently modified of the C23-C25-C27 triad. Digests of γS-C_0 produced fewer detectable mass shifted peptides. The observed shifts of +16 Da were observed for 2 peptides, corresponding to oxidation of M59 and M124. Why these two methionines are more readily oxidized than M74, M108 or M119 is yet unclear, given that

the latter residues all have a larger solvent accessible surface area. We speculate that local electrostatics are involved, however, further investigation is required.

Functional characterization of the interactions of *Ci-βγ* is highly relevant to understanding its role in the tunicate sensory vesicle. This structure, which contains both the ocellus and the otolith, is highly enriched in several metal cations, including Ca^{2+} and Zn^{2+} as a means of controlling its specific gravity.[4] We previously reported that the fluorescence intensity of *Ci-βγ* changes in response to Ca^{2+} binding, therefore, a preliminary analysis of fluorescence intensity changes was performed using Mg^{2+}, Sr^{2+}, Mn^{2+}, Co^{2+}, Ni^{2+}, and Zn^{2+} (Supplementary Figure S12). The changes in *Ci-βγ* fluorescence intensity were comparable to those observed upon binding Ca^{2+}, prompting us to continue with thermal unfolding and aggregation measurements. Interestingly, thermal aggregates of *apo-Ci-βγ* do not form until 60 °C, despite its thermal unfolding midpoint of 46 °C. The addition of divalent cations reverses this trend, resulting in a 10–15 °C lower T_m than T_i (Figure 5, Table 2). The persistence of this trend, independent of the degree of thermal stabilization, suggests that the underlying interactions of *Ci-βγ* with diffrent divalent cations are highly similar. Further, the diffrence in aggregate size between *apo-Ci-βγ* (< 50 nm) and cation bound *Ci-βγ* (>1000 nm) suggests that increased structural rigidity may alter the aggregation pathway.

Conclusion

The double clamp motif of the βγ-crystallin domain is capable of binding to a broad range of divalent cations beyond Ca^{2+}. This functionality is aided by the absence of readily oxidizable and cation-coordinating residues such as cysteine, histidine and methionine. In contrast, vertebrate lens γ-crystallins, which mostly do not bind divalent metal cations, are structurally similar but compositionally different. Notably the amino acid composition of the lens γ-crystallins favor more refractive residues, and their sequences were apparently not shaped by selective pressure against cysteines. In human γS-crystallin, solvent-exposed cysteine residues increase susceptibility to Zn^{2+}-induced aggregation through cross-linking, whereas Cu^{2+}-induced aggregation is driven by methionine oxidation.

Supplementary Material

Refer to Web version on PubMed Central for supplementary material.

Acknowledgement

The authors thank Dmitry Fishman for excellent management of the UCI Laser Spectroscopy Labs, Felix Grun and Ben Katz for excellent management of the Mass Spectrometry Facility, and Stephen White and Celia Goulding for access to the ITC instruments.

Funding

This work was supported by National Science Foundation Grants DMR-1410415 to R.W.M. and D.J. Tobias, DMS-1361425 to R.W.M. and C.T. Butts and National Institutes of Health Grant 1R01EY025328 to R.W.M. and D.J. Tobias. KWR was supported by National Science Foundation Grant DGE-1633631. R.W.M. is a CIFAR fellow.

References

(1). Wistow G; Summers L; Blundell T Myxococcus xanthus spore coat protein S may have a similar structure to vertebrate lens βγ-crystallins. Nature 1985, 315, 771–773. [PubMed: 3925350]

(2). Wistow G Evolution of a protein superfamily: relationships between vertebrate lens crystallins and microorganism dormancy proteins. Journal of Molecular Evolution 1990, 30, 140–145. [PubMed: 2107329]

(3). Esposito R; Racioppi C; Pezzotti M; Branno M; Locascio A; Ristoratore F; Spagnuolo A The ascidian pigmented sensory organs: Structures and developmental programs. Genesis: The Journal of Genetics and Development 2015, 53, 15–33.

(4). Sakurai D; Goda M; Kohmura Y; Horie T; Iwamoto H; Ohtsuki H; Tsuda M The role of pigment cells in the brain of ascidian larva. Journal of Comparative Neurology 2004, 475, 70–82. [PubMed: 15176085]

(5). Coniglio L; Morale A; Angelini C; Falugi C Cholinergic activation of settlement in Ciona intestinalis metamorphosing larvae. The Journal of Experimenal Zoology 1998, 280, 314–320.

(6). Shimeld SM; Purkiss AG; Dirks RP; Bateman OA; Slingsby C; Lubsen NH Urochordate βγ-crystallin and the evolutionary origin of the vertebrate eye lens. Current Biology 2005, 15, 1684–1689. [PubMed: 16169492]

(7). Khago D; Bierma JC; Roskamp KW; Kozlyuk N; Martin RW Protein refractive index increment is determined by conformation as well as composition. Journal of Physics: Condensed Matter 2018, 30, 435101. [PubMed: 30280702]

(8). Mishra A; Krishnan B; Raman R; Sharma Y Ca^{2+} and βγ-crystallins: An affair that did not last? Biochimica et Biophysica Acta - General Subjects 2016, 1860, 299–303.

(9). Slingsby C; Wistow GJ; Clark AR Evolution of crystallins for a role in the vertebrate eye lens. Protein Science 2013, 22, 367–380. [PubMed: 23389822]

(10). Barnwal RP; Jobby MK; Sharma Y; Chary KV NMR Assignment of M-crystallin: A Novel Ca^{2+} Binding Protein of the βγ-crystallin Superfamily from Methanosarcina acetivorans. Journal of Biomolecular NMR 2006, 36, 32–32. [PubMed: 16607466]

(11). Suman SK; Ravindra D; Sharma Y; Mishra A Association properties and unfolding of a βγ-crystallin domain of a Vibrio-specific protein. PloS One 2013, 8, e53610. [PubMed: 23349723]

(12). Jobby MK; Sharma Y Calcium-binding to lens βB2-and βA3-crystallins suggests that all β-crystallins are calcium-binding proteins. The FEBS Journal 2007, 274, 4135–4147. [PubMed: 17651443]

(13). Rajini B; Shridas P; Sundari CS; Muralidhar D; Chandani S; Thomas F; Sharma Y Calcium binding properties of γ-crystallin: calcium ion binds at the Greek key βγ-crystallin fold. Journal of Biological Chemistry 2001, 276, 38464–38471. [PubMed: 11502736]

(14). Kozlyuk N; Sengupta S; Bierma JC; Martin RW Calcium binding dramatically stabilizes an ancestral crystallin fold in tunicate βγ-crystallin. Biochemistry 2016, 55, 6961–6968. [PubMed: 27992995]

(15). Piatigorsky J Delta crystallins and their nucleic acids. Molecular and Cellular Biochemistry 1984, 59, 33–56. [PubMed: 6369110]

(16). Chiou S-H; Chang W; Chen C Characterization and comparison of epsilon-crystallin and lactate dehydrogenases in the lenses of vertebrates and invertebrates. Biochemistry International 1989, 18, 1093–1100. [PubMed: 2787637]

(17). Huang Q-L; Russell P; Stone S; Zigler J Zeta-crystallin, a novel lens protein from the guinea pig. Current Eye Research 1987, 6, 725–732. [PubMed: 3595182]

(18). Mulders J; Hendriks W; Blankesteijn WM; Bloemendal H; de Jong WW Lambda-crystallin, a major rabbit lens protein, is related to hydroxyacyl-coenzyme A dehydrogenases. Journal of Biological Chemistry 1988, 263, 15462–15466. [PubMed: 3170592]

(19). Wistow GJ; Lietman T; Williams LA; Stapel SO; De Jong WW; Horwitz J; Piatigorsky J Tau-crystallin/alpha-enolase: one gene encodes both an enzyme and a lens structural protein. The Journal of Cell Biology 1988, 107, 2729–2736. [PubMed: 2462567]

(20). Ghosh KS; Pande A; Pande J Binding of γ-crystallin substrate prevents the binding of copper and zinc ions to the molecular chaperone α-crystallin. Biochemistry 2011, 50, 3279–3281. [PubMed: 21417258]

(21). Copper and zinc ions specifically promote nonamyloid aggregation of the highly stable human γD-crystallin. ACS Chemical Biology 2015, 11, 263–272. [PubMed: 26579725]

(22). Ramkumar S; Fan X; Wang B; Yang S; Monnier VM Reactive cysteine residues in the oxidative dimerization and Cu^{2+} induced aggregation of human γD-crystallin: Implications for age-related cataract. Biochimica et Biophysica Acta - Molecular Basis of Disease 2018, 1864, 3595–3604. [PubMed: 30251679]

(23). Lin J Pathophysiology of cataracts: copper ion and peroxidation in diabetics. Japanese Journal of Ophthalmology 1997, 41, 130–137. [PubMed: 9243308]

(24). Aydin E; Cumurcu T; Özuğurlu F; Özyurt H; Sahinoglu S; Mendil D; Hasdemir E Levels of iron, zinc, and copper in aqueous humor, lens, and serum in nondiabetic and diabetic patients. Biological Trace Element Research 2005, 108, 33–41. [PubMed: 16327057]

(25). Cekic O Ėect of cigarette smoking on copper, lead, and cadmium accumulation in human lens. British Journal of Ophthalmology 1998, 82, 186–188. [PubMed: 9613387]

(26). Dawczynski J; Blum M; Winnefeld K; Strobel J Increased content of zinc and iron in human cataractous lenses. Biological Trace Element Research 2002, 90, 15–23. [PubMed: 12666821]

(27). Schmeling M; Gaynes BI; Tidow-Kebritchi S Heavy metal analysis in lens and aqueous humor of cataract patients by total reflection X-ray fluorescence spectrometry. Powder Di˙raction 2014, 29, 155–158.

(28). Domínguez-Calva J; Pérez-Vázquez M; Serebryany E; King J; Quintanar L Mercury-induced aggregation of human lens γ-crystallins reveals a potential role in cataract disease. Journal of Biological Inorganic Chemistry 2018, 23, 1105–1118. [PubMed: 30167892]

(29). Brazier MW; Davies P; Player E; Marken F; Viles JH; Brown DR Manganese binding to the prion protein. Journal of Biological Chemistry 2008, 283, 12831–12839. [PubMed: 18332141]

(30). Barnwal RP; Jobby M; Devi KM; Sharma Y; Chary KV Solution structure and calcium-binding properties of M-crystallin, a primordial βγ-crystallin from archaea. Journal of Molecular Biology 2009, 386, 675–689. [PubMed: 19138688]

(31). Aravind P; Mishra A; Suman SK; Jobby MK; Sankaranarayanan R; Sharma Y The βγ-crystallin superfamily contains a universal motif for binding calcium. Biochemistry 2009, 48, 12180–12190. [PubMed: 19921810]

(32). Kretschmar M; Mayr E-M; Jaenicke R Kinetic and thermodynamic stabilization of the βγ-crystallin homolog spherulin 3a from P hysarum polycephalum by calcium binding. Journal of Molecular Biology 1999, 289, 701–705. [PubMed: 10369756]

(33). Wenk M; Baumgartner R; Holak TA; Huber R; Jaenicke R; Mayr E-M The domains of protein S from Myxococcus xanthus: structure, stability and interactions. Journal of Molecular Biology 1999, 286, 1533–1545. [PubMed: 10064714]

(34). Riyahi K; Shimeld SM Chordate βγ-crystallins and the evolutionary developmental biology of the vertebrate lens. Comparative Biochemistry and Physiology Part B: Biochemistry and Molecular Biology 2007, 147, 347–357.

(35). Snyder EE; Buoscio BW; Falke JJ Calcium (II) site specificity: effect of size and charge on metal ion binding to an EF-hand-like site. Biochemistry 1990, 29, 3937–3943. [PubMed: 2162201]

(36). Park C-S; MacKinnon R Divalent cation selectivity in a cyclic nucleotide-gated ion channel. Biochemistry 1995, 34, 13328–13333. [PubMed: 7577917]

(37). Brunet S; Scheuer T; Klevit R; Catterall WA Modulation of CaV1. 2 channels by Mg^{2+} acting at an EF-hand motif in the COOH-terminal domain. The Journal of General Physiology 2005, 126, 311–323. [PubMed: 16157690]

(38). Dove S; Kingsford M Use of otoliths and eye lenses for measuring trace-metal incorporation in fishes: a biogeographic study. Marine Biology 1998, 130, 377–387.

(39). Clout NJ; Kretschmar M; Jaenicke R; Slingsby C Crystal structure of the calcium-loaded spherulin 3a dimer sheds light on the evolution of the eye lens βγ-crystallin domain fold. Structure 2001, 9, 115–124. [PubMed: 11250196]

(40). Vergara A; Grassi M; Sica F; Pizzo E; D'Alessio G; Mazzarella L; Merlino A A novel interdomain interface in crystallins: structural characterization of the βγ-crystallin from Geodia cydonium at 0.99 Å resolution. Acta Crystallographica Section D 2013, 69, 960–967.

(41). Kumar S; Stecher G; Tamura K MEGA7: molecular evolutionary genetics analysis version 7.0 for bigger datasets. Molecular Biology and Evolution 2016, 33, 1870–1874. [PubMed: 27004904]

(42). Edgar RC MUSCLE: multiple sequence alignment with high accuracy and high throughput. Nucleic acids research 2004, 32, 1792–1797. [PubMed: 15034147]

(43). Pond SLK; Muse SV Statistical Methods in Molecular Evolution; Springer, 2005; pp 125–181.

(44). Willard L; Ranjan A; Zhang H; Monzavi H; Boyko RF; Sykes BD; Wishart DS VADAR: a web server for quantitative evaluation of protein structure quality. Nucleic Acids Research 2003, 31, 3316–3319. [PubMed: 12824316]

(45). Ebersbach H; Fiedler E; Scheuermann T; Fiedler M; Stubbs MT; Reimann C; Proetzel G; Rudolph R; Fiedler U Affilin–novel binding molecules based on human γ-B-Crystallin, an all β-sheet protein. Journal of Molecular Biology 2007, 372, 172–185. [PubMed: 17628592]

(46). Dixit K; Pande A; Pande J; Sarma SP Nuclear Magnetic Resonance Structure of a Major Lens Protein, Human γC-Crystallin: Role of the Dipole Moment in Protein Solubility. Biochemistry 2016, 55, 3136–3149. [PubMed: 27187112]

(47). Basak A; Bateman O; Slingsby C; Pande A; Asherie N; Ogun O; Benedek GB; Pande J High-resolution X-ray crystal structures of human γD crystallin (1.25 Å) and the R58H mutant (1.15 Å) associated with aculeiform cataract. Journal of Molecular Biology 2003, 328, 1137–1147. [PubMed: 12729747]

(48). Brubaker WD; Martin RW ^{1}H, ^{13}C, and ^{15}N assignments of wild-type human γS-crystallin and its cataract-related variant γS-G18V. Biomolecular NMR Assignments 2012, 6, 63–67. [PubMed: 21735120]

(49). Zhang Y I-TASSER server for protein 3D structure prediction. BMC bioinformatics 2008, 9, 40. [PubMed: 18215316]

(50). Studier FW Protein production by auto-induction in high-density shaking cultures. Protein Expression and Purification 2005, 41, 207–234. [PubMed: 15915565]

(51). Thorn DC; Grosas AB; Mabbitt PD; Ray NJ; Jackson CJ; Carver JA The structure and stability of the disulfide-linked γS-crystallin dimer provide insight into oxidation products associated with lens cataract formation. Journal of Molecular Biology 2019, 431, 483–497. [PubMed: 30552875]

(52). Hains PG; Truscott RJ Post-translational modifications in the nuclear region of young, aged, and cataract human lenses. Journal of Proteome Research 2007, 6, 3935–3943. [PubMed: 17824632]

(53). Wilmarth P; Tanner S; Dasari S; Nagalla S; Riviere M; Bafna V; Pevzner P; David L Age-related changes in human crystallins determined from comparative analysis of post-translational modifications in young and aged lens: does deamidation contribute to crystallin insolubility? Journal of Proteome Research 2006, 5, 2554–2566. [PubMed: 17022627]

(54). Madian AG; Regnier FE Proteomic identification of carbonylated proteins and their oxidation sites. Journal of Proteome Research 2010, 9, 3766–3780. [PubMed: 20521848]

(55). Pitt AR; Spickett CM Mass spectrometric analysis of HOCl-and free-radical-induced damage to lipids and proteins. Biochemical Society Transactions 2008, 36, 1077–1082. [PubMed: 18793192]

(56). Sun H; Ma Z; Li Y; Liu B; Li Z; Ding X; Gao Y; Ma W; Tang X; Li X; Shen Y Gamma-S crystallin gene (CRYGS) mutation causes dominant progressive cortical cataract in humans. Journal of Medical Genetics 2005, 42, 706–710. [PubMed: 16141006]

(57). Devi RR; Yao W; Vijayalakshmi P; Sergeev YV; Sundaresan P; Hejtmancik JF Crystallin gene mutations in Indian families with inherited pediatric cataract. Molecular Vision 2008, 14, 1157–1170. [PubMed: 18587492]

(58). Vendra VPR; Khan I; Chandani S; Muniyandi A; Balasubramanian D Gamma crystallins of the human eye lens. Biochimica et Biophysica Acta - General Subjects 2016, 1860, 333–343.

(59). Ji F; Jung J; Gronenborn AM Structural and biochemical characterization of the childhood cataract-associated R76S mutant of human γD-crystallin. Biochemistry 2012, 51, 2588–2596. [PubMed: 22394327]

(60). Suman SK; Mishra A; Ravindra D; Yeramala L; Sharma Y Evolutionary remodelling of the betagamma-crystallins for domain stability at the cost of Ca^{2+}- binding. Journal of Biological Chemistry 2011, 8, jbc–M111.

(61). Suman SK; Mishra A; Yeramala L; Rastogi ID; Sharma Y Disability for function: loss of Ca^{2+}-binding is obligatory for fitness of mammalian βγ-crystallins. Biochemistry 2013, 52, 9047–9058. [PubMed: 24251594]

(62). Srivastava SS; Mishra A; Krishnan B; Sharma Y Ca^{2+}-binding Motif of βγ-Crystallins. Journal of Biological Chemistry 2014, 289, 10958–10966. [PubMed: 24567326]

(63). Kozlov K Vertebrate Crystallins–from Proteins to Genes. Russian Journal of Developmental Biology 2001, 32, 265–282.

(64). Wistow G The human crystallin gene families. Human Genomics 2012, 6, 26. [PubMed: 23199295]

(65). Shu N; Zhou T; Hovmöller S Prediction of zinc-binding sites in proteins from sequence. Bioinformatics 2008, 24, 775–782. [PubMed: 18245129]

(66). Keenan J; Orr D; Pierscionek B Patterns of crystallin distribution in porcine eye lenses. Molecular Vision 2008, 14, 1245–1253. [PubMed: 18615203]

(67). Chen Y; Zhao H; Schuck P; Wistow G Solution properties of γ-crystallins: Compact structure and low frictional ratio are conserved properties of diverse γ-crystallins. Protein Science 2014, 23, 76–87. [PubMed: 24214907]

(68). Zhao H; Brown PH; Schuck P On the distribution of protein refractive index increments. Biophysical Journal 2011, 100, 2309–2317. [PubMed: 21539801]

(69). Serebryany E; Yu S; Trauger SA; Budnik B; Shakhnovich EI Dynamic disulfide exchange in a crystallin protein in the human eye lens promotes cataract-associated aggregation. Journal of Biological Chemistry 2018, 293, 17997–18009. [PubMed: 30242128]

(70). Lapko VN; Smith DL; Smith JB Methylation and carbamylation of human γ-crystallins. Protein Science 2003, 12, 1762–1774. [PubMed: 12876325]

(71). Kosakovsky Pond SL; Frost SD Not so different after all: a comparison of methods for detecting amino acid sites under selection. Molecular Biology and Evolution 2005, 22, 1208–1222. [PubMed: 15703242]

(72). Senguen FT; Grabarek Z X-ray structures of magnesium and manganese complexes with the N-terminal domain of calmodulin: insights into the mechanism and specificity of metal ion binding to an EF-hand. Biochemistry 2012, 51, 6182–6194. [PubMed: 22803592]

(73). Lewit-Bentley A; Réty S EF-hand calcium-binding proteins. Current Opinion in Structural Biology 2000, 10, 637–643. [PubMed: 11114499]

(74). Fukuda M; Kojima T; Mikoshiba K Regulation by bivalent cations of phospholipid binding to the C2A domain of synaptotagmin III. Biochemical Journal 1997, 323, 421–425. [PubMed: 9163333]

(75). Teintze M; Inouye M; Inouye S Characterization of calcium-binding sites in development-specific protein S of Myxococcus xanthus using site-specific mutagenesis. Journal of Biological Chemistry 1988, 263, 1199–1203. [PubMed: 3121626]

(76). Jobby MK; Sharma Y Calcium-binding crystallins from Y ersinia pestis: characterization of two single βγ-crystallin domains of a putative exported protein. Journal of Biological Chemistry 2005, 280, 1209–1216. [PubMed: 15536081]

(77). Feng M; Patel D; Dervan J; Ceska T; Suck D; Haq I; Sayers J Roles of divalent metal ions in flap endonuclease–substrate interactions. Nature Structural and Molecular Biology 2004, 11, 450–456.

(78). Chao Y; Fu D Thermodynamic studies of the mechanism of metal binding to the Escherichia coli zinc transporter YiiP. Journal of Biological Chemistry 2004, 279, 17173–17180. [PubMed: 14960568]

(79). Basak P; Debnath T; Banerjee R; Bhattacharyya M Selective binding of divalent cations toward heme proteins. Frontiers in Biology 2016, 11, 32–42.

(80). Huang X; Miller W A time-efficient, linear-space local similarity algorithm. Advances in Applied Mathematics 1991, 12, 337–357.

(81). Bodenhausen G; Ruben D Natural abundance nitrogen-15 NMR by enhanced heteronuclear spectroscopy. Chemical Physics Letters 1980, 69, 185–189.

(82). Nara M; Tanokura M; Yamamoto T; Tasumi M A comparative study of the binding effects of Mg^{2+}, Ca^{2+}, Sr^{2+}, and Cd^{2+} on calmodulin by fourier-transform infrared spectroscopy. Biospectroscopy 1995, 1, 47–54.

(83). Chao SH; Suzuki Y; Zysk JR; Cheung W Activation of calmodulin by various metal cations as a function of ionic radius. Molecular Pharmacology 1984, 26, 75–82. [PubMed: 6087119]

(84). Ozawa T; Sasaki K; Umezawa Y Metal ion selectivity for formation of the calmodulin–metal–target peptide ternary complex studied by surface plasmon resonance spectroscopy. Biochimica et Biophysica Acta - Protein Structure and Molecular Enzymology 1999, 1434, 211–220.

(85). Yamniuk AP; Nguyen LT; Hoang TT; Vogel HJ Metal ion binding properties and conformational states of calcium-and integrin-binding protein. Biochemistry 2004, 43, 2558–2568. [PubMed: 14992593]

(86). Yamniuk AP; Silver DM; Anderson KL; Martin SR; Vogel HJ Domain stability and metal-induced folding of calcium-and integrin-binding protein 1. Biochemistry 2007, 46, 7088–7098. [PubMed: 17516631]

(87). Blancuzzi Y; Padilla A; Cave A; Parello J Symmetrical rearrangement of the cation-binding sites of parvalbumin upon calcium/magnesium exchange. A study by proton 2D NMR. Biochemistry 1993, 32, 1302–1309. [PubMed: 8095405]

(88). Kosinski-Collins MS; Flaugh SL; King J Probing folding and fluorescence quenching in human γD crystallin Greek key domains using triple tryptophan mutant proteins. Protein Science 2004, 13, 2223–2235. [PubMed: 15273315]

(89). Flaugh SL; Kosinski-Collins MS; King J Contributions of hydrophobic domain interface interactions to the folding and stability of human γD-crystallin. Protein Science 2005, 14, 569–581. [PubMed: 15722442]

(90). Ma Z; Piszczek G; Wingfield PT; Sergeev YV; Hejtmancik JF The G18V CRYGS mutation associated with human cataracts increases γS-crystallin sensitivity to thermal and chemical stress. Biochemistry 2009, 48, 7334–7341. [PubMed: 19558189]

(91). Brubaker WD; Freites JA; Golchert KJ; Shapiro RA; Morikis V; Tobias DJ; Martin RW Separating instability from aggregation propensity in γS-crystallin variants. Biophysical Journal 2011, 100, 498–506. [PubMed: 21244846]

(92). Ray D, Nicholas Jand Hall; Carver, J. A. Deamidation of N76 in human γS-crystallin promotes dimer formation. Biochimica et Biophysica Acta (BBA) - General Subjects 2016, 1860, 315–324. [PubMed: 26318015]

(93). Khrustalev VV; Barkovsky EV; Khrustaleva TA Magnesium and manganese binding sites on proteins have the same predominant motif of secondary structure. Journal of Theoretical Biology 2016, 395, 174–185. [PubMed: 26876751]

(94). Shannon RD Revised effective ionic radii and systematic studies of interatomic distances in halides and chalcogenides. Acta Crystallographica Section A 1976, 32, 751–767.

(95). Pearson RG Hard and soft acids and bases. Journal of the American Chemical Society 1963, 85, 3533–3539.

(96). Hsin K; Sheng Y; Harding M; Taylor P; Walkinshaw M MESPEUS: a database of the geometry of metal sites in proteins. Journal of Applied Crystallography 2008, 41, 963–968.

(97). Dudev M; Wang J; Dudev T; Lim C Factors governing the metal coordination number in metal complexes from Cambridge Structural Database analyses. The Journal of Physical Chemistry B 2006, 110, 1889–1895. [PubMed: 16471760]

(98). Harding MM Geometry of metal–ligand interactions in proteins. Acta Crystallographica Section D 2001, 57, 401–411.

(99). Banerjee PR; Pande A; Shekhtman A; Pande J Molecular mechanism of the chaperone function of mini-α-crystallin, a 19-residue peptide of human α-crystallin. Biochemistry 2014, 54, 505–515. [PubMed: 25478825]

(100). Khago D; Wong EK; Kingsley CN; Freites JA; Tobias DJ; Martin RW Increased hydrophobic surface exposure in the cataract-related G18V variant of human γS-crystallin. Biochimica et Biophysica Acta (BBA)-General Subjects 2016, 1860, 325–332. [PubMed: 26459004]

(101). Domínguez-Calva JA; Haase-Pettingell C; Serebryany E; King JA; Quintanar L A histidine switch for Zn-induced aggregation of γ-crystallins reveals a metal-bridging mechanism relevant to cataract disease. Biochemistry 2018, 57, 4959–4962. [PubMed: 30064223]

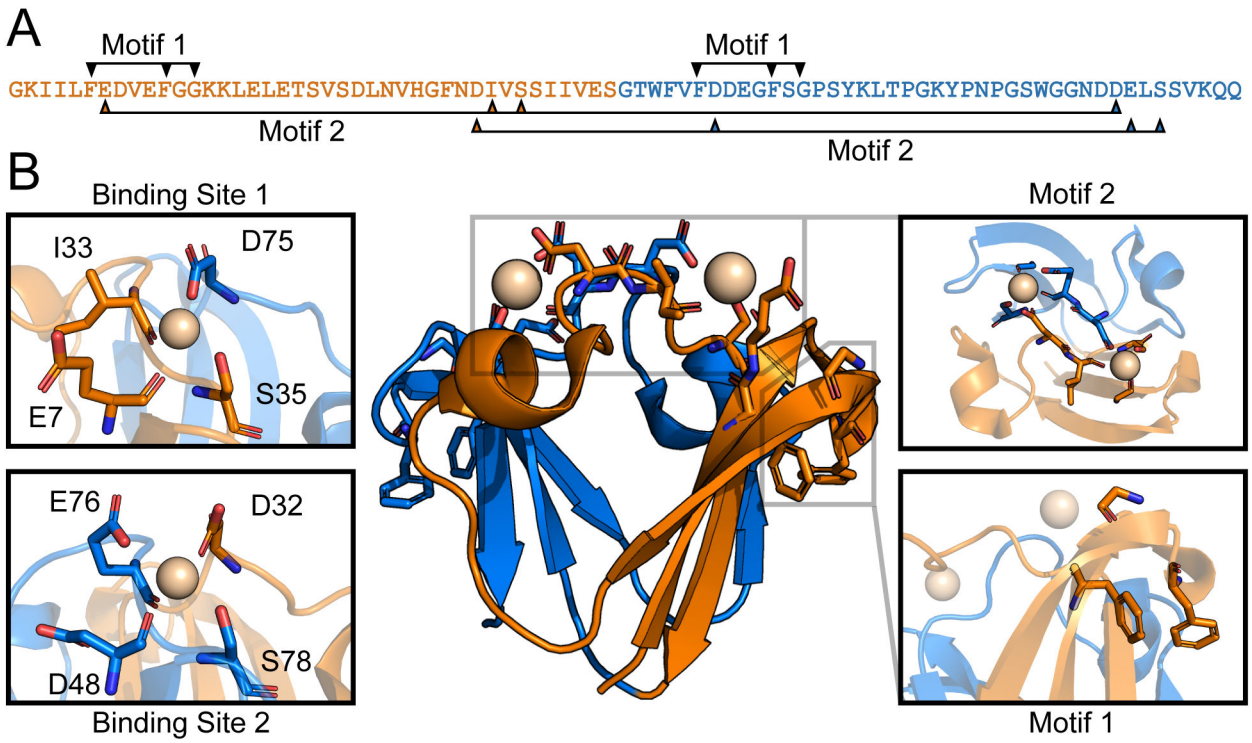

Figure 1:

(A) The sequence of *Ci*-$\beta\gamma$-crystallin annotated with the residues comprising the (F/Y/W)xxxx(F/Y)xG (motif 1) and cation-binding site (motif 2). The residues of the first Greek key are colored orange; those of the second Greek key are colored blue. (B) Both motifs are visualized within the calcium-bound X-ray crystal structure of *Ci*-$\beta\gamma$ (PDBID: 2BV2).[6] Secondary images are displayed on the right for clarity. The residues comprising the first and second binding site are displayed to the left. The first binding site is made up of the D75 sidechain carboxylate, S35 sidechain hydroxyl, E7 backbone carbonyl, and I33 backbone carbonyl. The second binding site is made up of the D32 sidechain acid, S78 sidechain hydroxyl, E48 backbone carbonyl, E76 backbone carbonyl and E76 sidechain carboxylate.

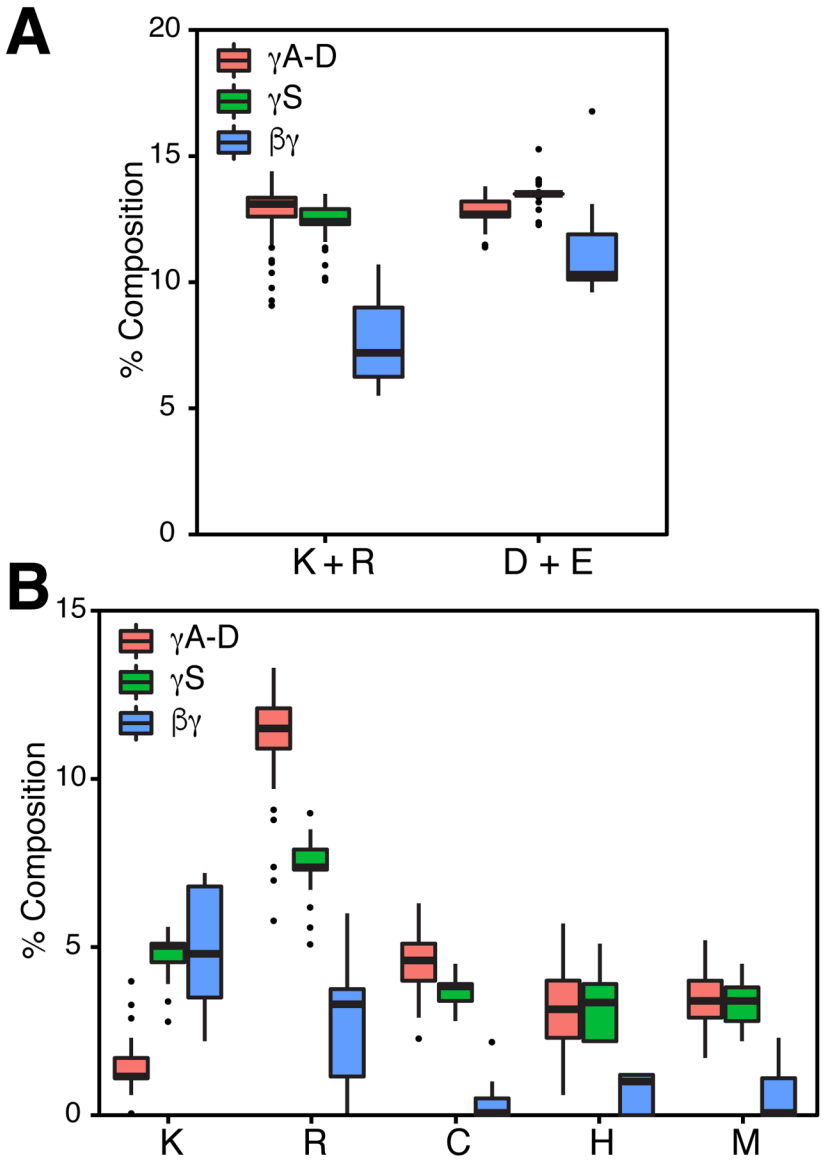

Figure 2:

Combined and individual amino acid sequence percentages of lens γA-D (red), lens γS (green), and cation-binding $\beta\gamma$-crystallins (blue). Each box covers the 25th to 75th percentiles and whiskers extend to 1.5 times the largest value in the respective quartile range. (A) Percentages of positively charged (lysine and arginine) and negatively charged (aspartate and glutamate) residues. (B) Lysine, arginine, cysteine, histidine, and methionine sequence percentage of each group.

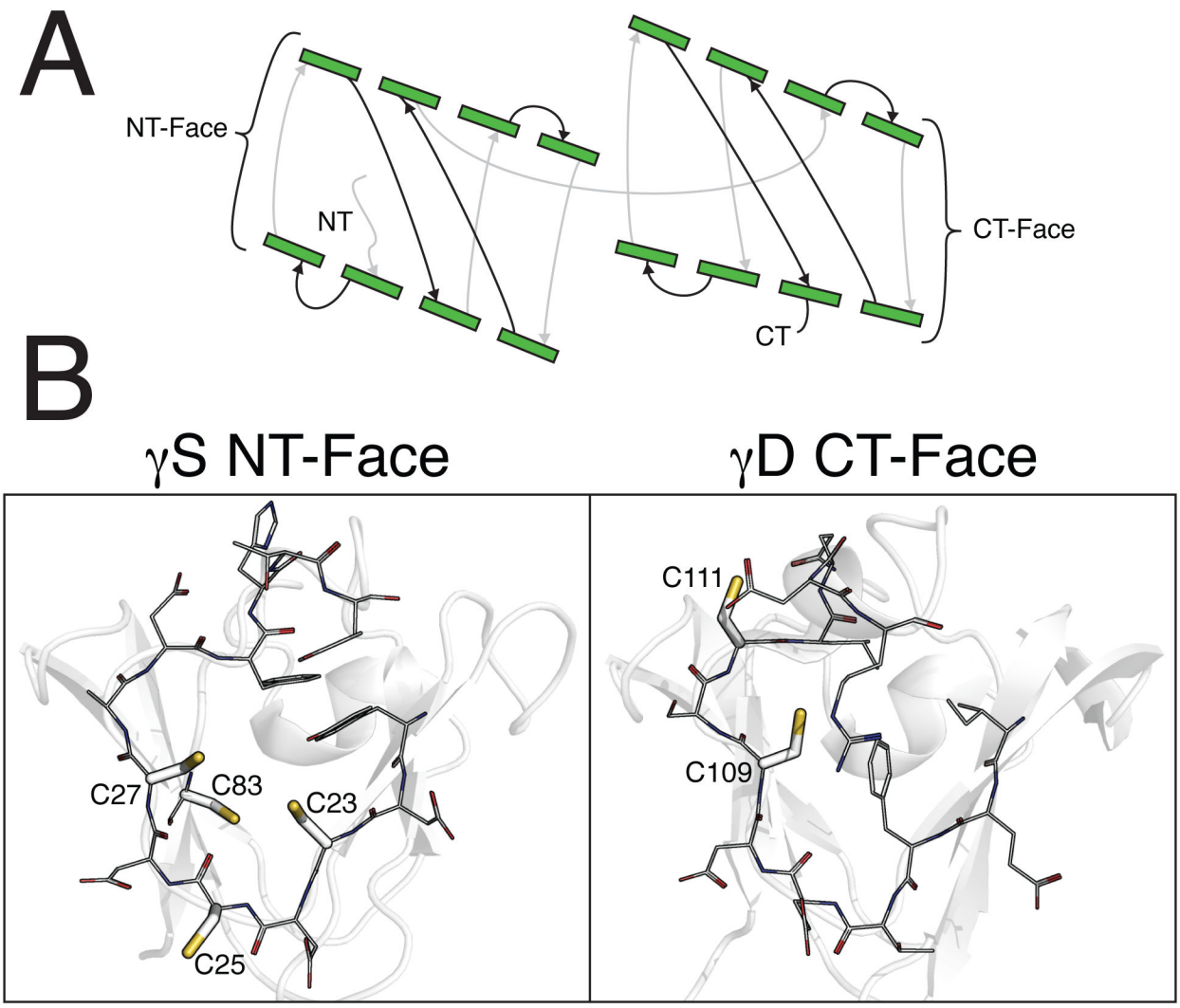

Figure 3:

(A) A schematic of the γ-crystallin structure showing the location of the external β-sandwich faces of the N-terminal and C-terminal domains. The β-strands of the protein are shown as green rectangles lines drawn between them to illustrate the relative strand connectivity (black - top, gray - bottom). (B) The ribbon structure of N-terminal face of γS (PDBID: 2M3T[48]) and and C-terminal face of γD-crystallin (PDBID: 1HK0[47]) are shown overlaid with line renderings of relevant residues. The cysteines of both faces are shown as sticks. γS-C83 is depicted in γS-NT face due to its proximity despite being located one β-strand behind the N-terminal face.

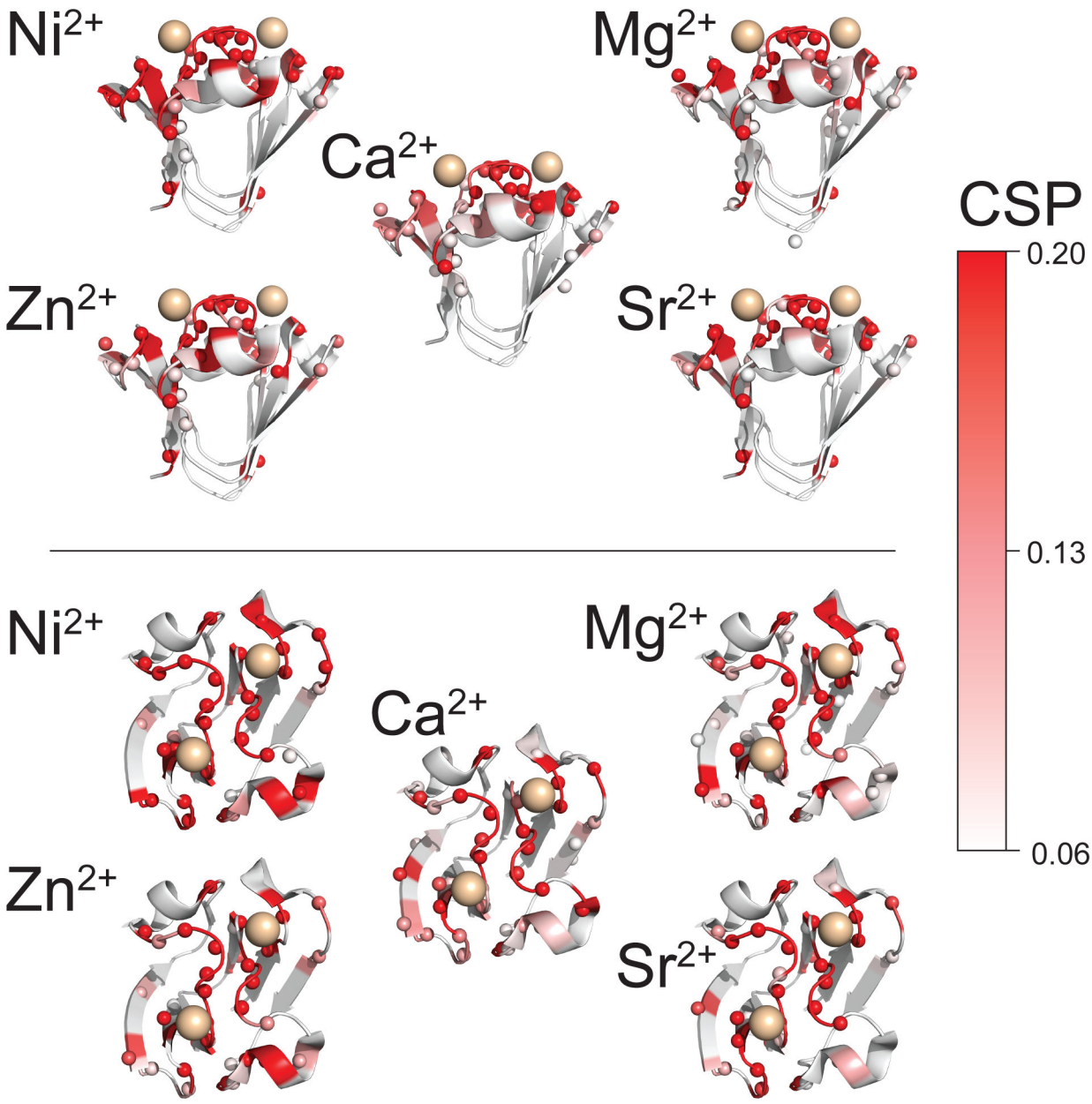

Figure 4:

1H-^{15}N-HSQC CSPs of *Ci-βγ* resulting from the addition of 6.5 equivalents of Ca^{2+}, Sr^{2+}, Mg^{2+}, Ni^{2+}, and Zn^{2+} were mapped onto the structure of *Ci-βγ* (PDBID: 2BV2). Weak CSPs (≤ 0.06) are colored white, strong CSPs (≥ 0.2) are colored red, and moderate CSPs are colored using a red to white gradient. The color gradient is projected onto the cartoon backbone and the spheres representing backbone amide nitrogens. Ca^{2+} ions found in the crystal structure are represented as tan spheres.

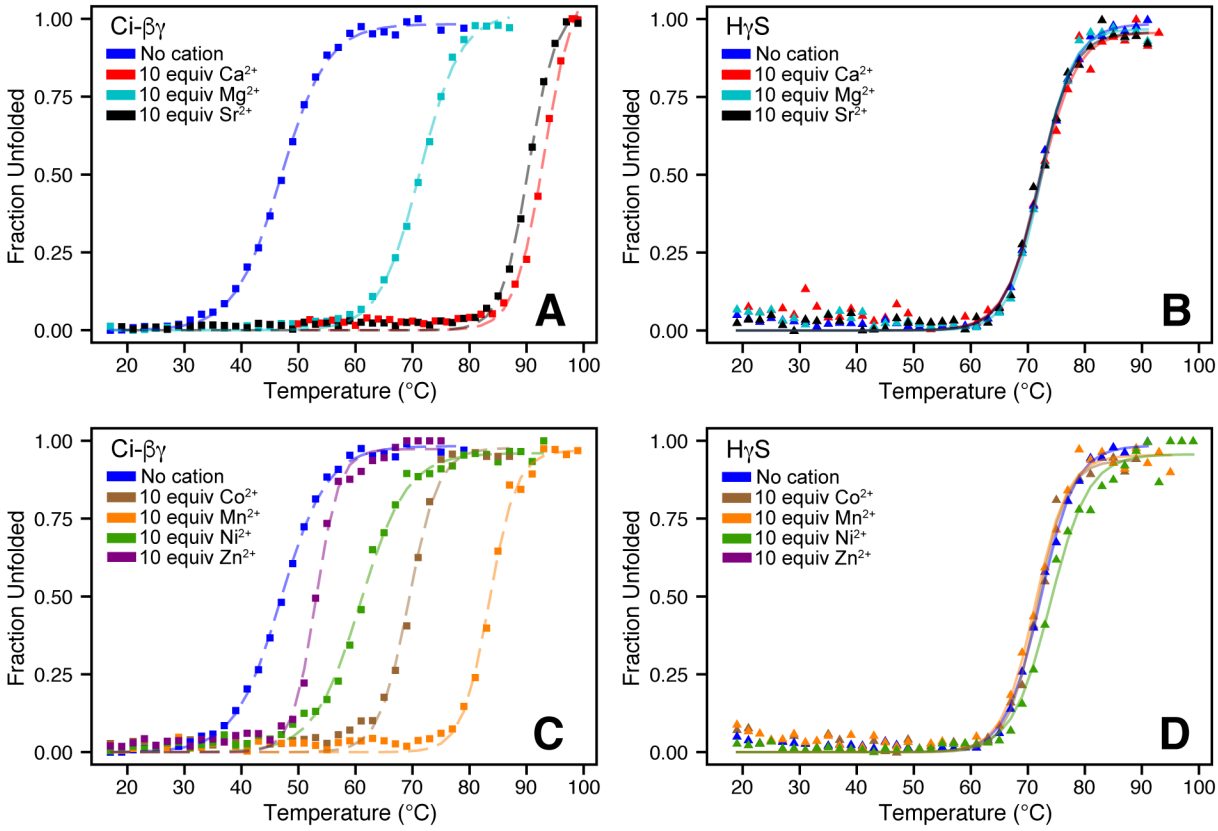

Figure 5:

Protein thermal unfolding in the presence of 10 equivalents of divalent cation. (A) *Ci-βγ* in the presence of Ca^{2+} (red), Mg^{2+} (aqua), Sr^{2+} (black), or no cation (blue). (B) HγS in the presence of Ca^{2+} (red), Mg^{2+} (aqua), Sr^{2+} (black), or no cation (blue). (C) *Ci-βγ* in the presence of Co^{2+} (brown), Mn^{2+} (orange), Ni^{2+} (green), Zn^{2+} (purple), or no cation (blue). (D) HγS in the presence of Co^{2+} (brown), Mn^{2+} (orange), Ni^{2+} (green), or no cation (blue).

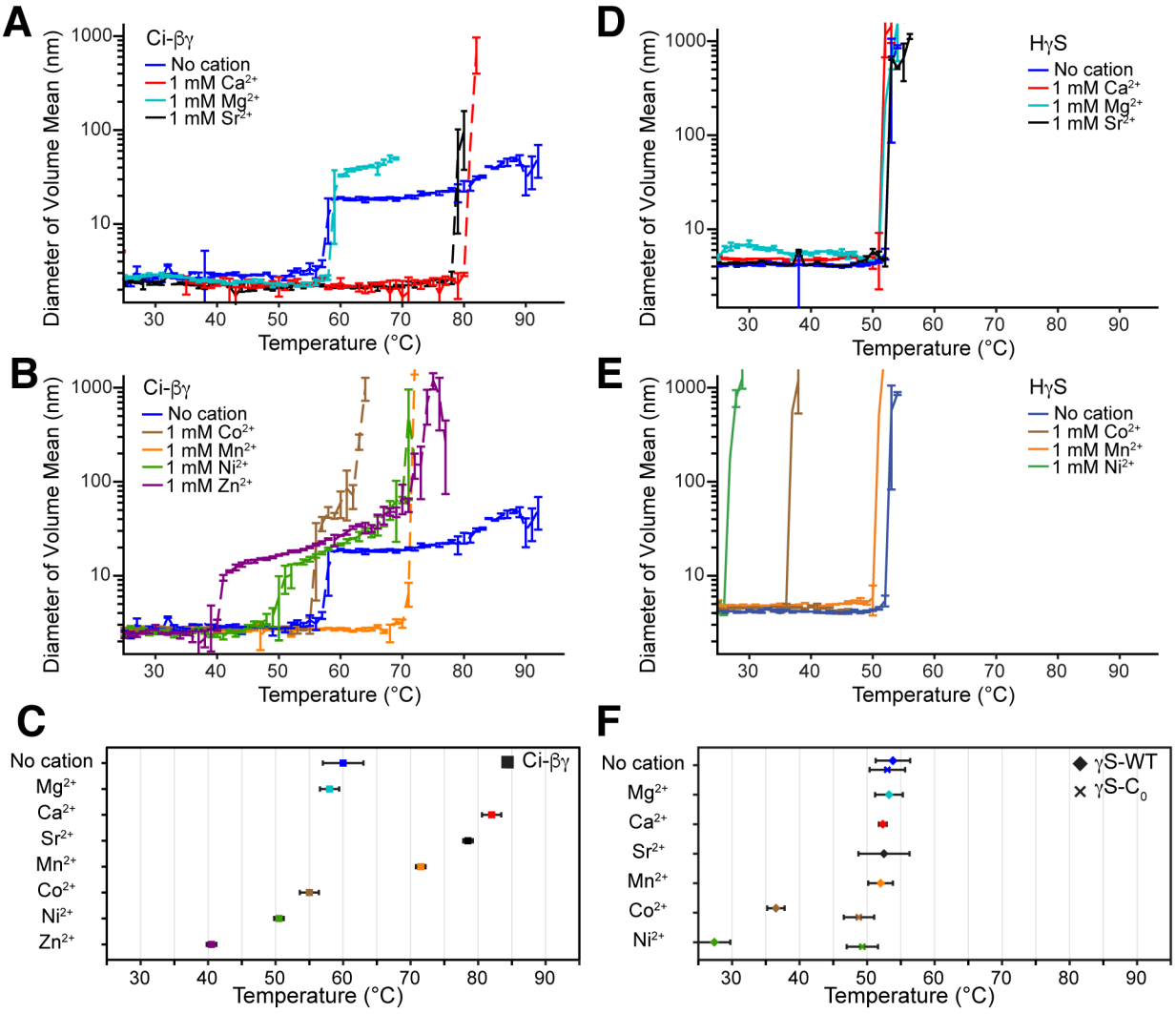

Figure 6:

DLS was used to monitor the diameter of protein monomers and oligomers to access the temperature of aggregate formation under thermal stress and in the presence of 10 equivalents of divalent cation. (A) DLS measurements for *Ci-βγ* in the presence of Ca^{2+} (red), Mg^{2+} (aqua), Sr^{2+} (black), or no cation (blue). (B) DLS of *Ci-βγ* in the presence of Co^{2+} (brown), Mn^{2+} (orange), Ni^{2+} (green), Zn^{2+} (purple), or no cation (blue). Each measurement trace reflects one representative measurement, where error bars correspond to one standard deviation collected from triplicate sampling at each temperature. (C) The initial temperature of oligomer formation (T_i) for *Ci-βγ* under thermal stress measured via DLS. The T_i refers to the lowest temperature at which species larger than the native monomers are observed. This plot is derived from the data shown in Panels (A) and (B); this alternative visualization facilitates comparison of the aggregation onset temperatures and allows more straightforward presentation of the measurement error. Error bars represent one standard deviation. (D) DLS for HγS in the presence of Ca^{2+} (red), Mg^{2+} (aqua), Sr^{2+} (black), or no cation (blue). (E) DLS of HγS in the presence of Co^{2+} (brown), Mn^{2+} (orange), Ni^{2+}

(green), or no cation (blue). *Ci-βγ* (top), were measured (E) The initial temperature of oligomer formation (T_i) for HγS (diamonds), and HγS-C_0 (Xs), presented as in Panel (C)

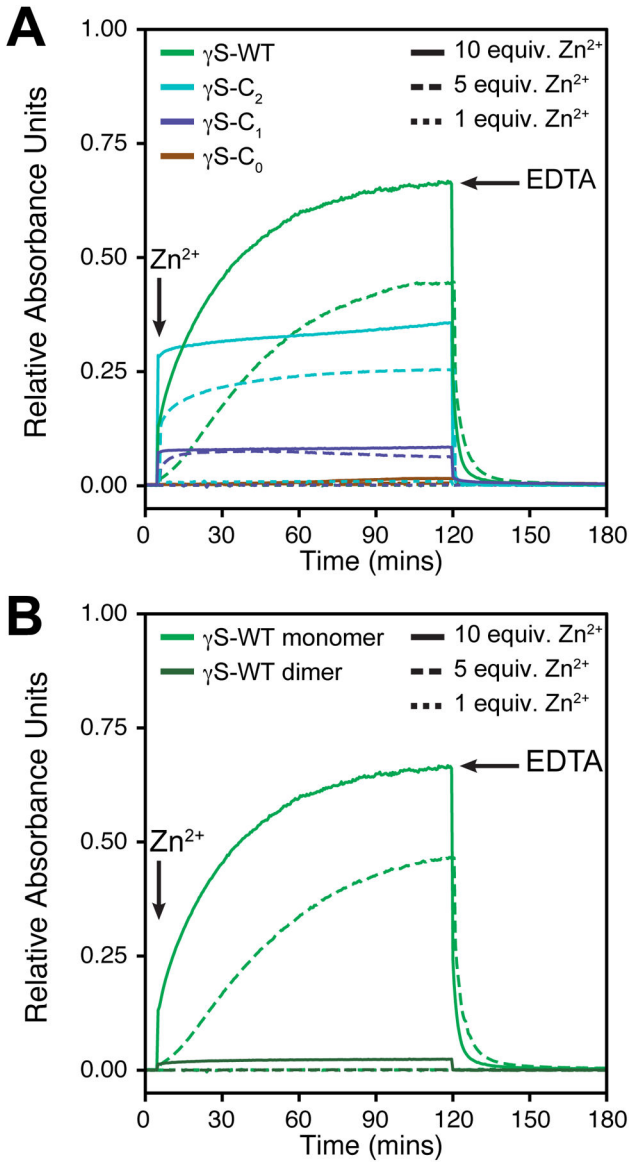

Figure 7:

Treatment of human γS-crystallin and its cysteine-to-serine variants with 1 (small dashed lines), 5 (long dashed lines) or 10 (solid lines) equivalents of Zn^{2+}. (A) Light scattering of monomeric HγS wild-type (green), HγS-C_2 (cyan), HγS-C_1 (purple), and HγS-C_0 (brown). (B) Light scattering of monomeric HγS (green) and dimeric HγS (dark green). The HγS wild-type dimer was collected from the protein purification process without further modification.

Table 1:

Thermodynamic parameters for binding of Ca^{2+} and Sr^{2+} to *Ci-βγ*.

	K **(M^{-1})**	**ΔH (kJ/mol)**	**ΔG (kJ/mol)**	**−TΔS (kJ/mol)**
Ca^{2+} Site 1	$3.5 \times 10^8 \pm 2.2 \times 10^8$	−26.6±6.5	−48.5±1.7	−21.9±8.7
Ca^{2+} Site 2	$5.9 \times 10^7 \pm 1.2 \times 10^7$	−21.9±0.8	−44.4±0.5	−22.5±0.3
Sr^{2+} Site 1	$1.2 \times 10^8 \pm 1.8 \times 10^7$	−31.6±2.3	−46.0±0.4	−14.4±2.5
Sr^{2+} Site 2	$5.6 \times 10^6 \pm 3.2 \times 10^6$	−18.5±1.7	−38.3±1.6	−19.8±3.3

Table 2:

Divalent cations classification and effect on *Ci-βγ* unfolding.

	T_m[2]	T_i[3]	Ionic radius[4]	Classification[5]	MESPUES CN[6]	CSD CN[7]
Ca^{2+}	94° C	82°C	100 pm	Hard	6–8	6, 7
Sr^{2+}	91°C	79° C	118 pm	Hard	-	6, 8
Mn^{2+}	84° C	72°C	83 pm[8]	Borderline	6	6
Mg^{2+}	71°C	58°C	72 pm	Hard	6	6
Co^{2+}	70° C	55°C	74.5pm[9]	Borderline	6	4, 6
Ni^{2+}	61°C	50°C	69 pm	Borderline	4	4, 6
Zn^{2+}	53°C	40°C	74 pm	Borderline	4[10]	4
Apo	46° C	60°C	-	-	-	

[2]Thermal denaturation midpoint (T_m) determined via intrinsic fluorescence.

[3]Initial temperature of aggregation (T_i) determined via DLS.

[4]All ionic radius values are taken from Shannon *et al*.[94] using the 6-coordinate, 2+ charge state.

[5]From Pearson's classification of hard and soft acids and bases.[95]

[6]Coordination number (CN) collected from MESPEUS 10 and Hsin *et al*.[96]

[7]Coordination number (CN) taken from Dudev *et al*,[97] Tables 1, 2, and 3 for frequencies 33 %.

[8]High-spin ionic radius.

[9]High-spin ionic radius.

[10]Taken form Harding *et al*,[98] Table 5.